ANNALS of Clinical and Translational Neurology
Open Access
ANA American Neurological Association since 1875

RESEARCH ARTICLE

# Altered *PLP1* splicing causes hypomyelination of early myelinating structures

Sietske H. Kevelam[1,2,a], Jennifer R. Taube[3,a], Rosalina M. L. van Spaendonk[4,a], Enrico Bertini[5], Karen Sperle[3], Mark Tarnopolsky[6], Davide Tonduti[7], Enza Maria Valente[8,9], Lorena Travaglini[5], Erik A. Sistermans[4], Geneviève Bernard[10], Coriene E. Catsman-Berrevoets[11], Clara D. M. van Karnebeek[12], John R. Østergaard[13], Richard L. Friederich[14], Mahmoud Fawzi Elsaid[15], Jolanda H. Schieving[16], Maja Tarailo-Graovac[17], Simona Orcesi[18], Marjan E. Steenweg[1,2], Carola G. M. van Berkel[1], Quinten Waisfisz[4], Truus E. M. Abbink[1,2], Marjo S. van der Knaap[1,2,19], Grace M. Hobson[3,20,21,b] & Nicole I. Wolf[1,2,b]

[1]Department of Child Neurology, VU University Medical Center, Amsterdam, The Netherlands
[2]Neuroscience Campus Amsterdam, VU University, Amsterdam, The Netherlands
[3]Nemours Biomedical Research, Alfred I. duPont Hospital for Children, Wilmington, Delaware
[4]Department of Clinical Genetics, VU University Medical Center, Amsterdam, The Netherlands
[5]Unit for Neuromuscular and Neurodegenerative Diseases, Laboratory of Molecular Medicine, Bambino Gesu' Children's Research Hospital, IRCCS, Rome, Italy
[6]Department of Pediatrics, McMaster Children's Hospital, Hamilton, Ontario, Canada
[7]Child Neuropsychiatry Unit, Department of Brain and Behavioral Sciences, University of Pavia, Pavia, Italy
[8]Department of Medicine and Surgery, University of Salerno, Salerno, Italy
[9]CSS-Mendel Institute, IRCCS Casa Sollievo della Sofferenza, San Giovanni Rotondo, Italy
[10]Division of Pediatric Neurology, Departments of Pediatrics, Neurology and Neurosurgery, Montreal Children's Hospital, McGill University Health Center, Montreal, Quebec, Canada
[11]Department of Pediatric Neurology, Erasmus University Hospital – Sophia Children's Hospital, Rotterdam, The Netherlands
[12]Division of Biochemical Diseases, Department of Pediatrics, BC Children's Hospital, Centre for Molecular Medicine and Therapeutics, University of British Columbia, Vancouver, Canada
[13]Centre for Rare diseases, Department of Paediatrics, Aarhus University Hospital, Aarhus, Denmark
[14]Department of Child Neurology, Kaiser Permanente Pediatric Specialties, Roseville, California
[15]Department of Pediatric Neurology, Hamad Medical Corp, Doha, Qatar
[16]Department of Child Neurology, Radboud University Medical Center, Nijmegen, The Netherlands
[17]Department of Medical Genetics, University of British Colombia, Vancouver, Canada
[18]Child Neurology and Psychiatry Unit, C. Mondino National Neurological Institute, Pavia, Italy
[19]Department of Functional Genomics, Center for Neurogenomics and Cognitive Research, VU University, Amsterdam, The Netherlands
[20]Department of Biological Sciences, University of Delaware, Newark, Delaware
[21]Department of Pediatrics, Jefferson Medical College, Thomas Jefferson University, Philadelphia, Pennsylvania

**Correspondence**
Nicole I. Wolf, Department of Child Neurology, VU University Medical Center, De Boelelaan 1117, 1081 HV Amsterdam, The Netherlands. Tel: +31-20-44 40859; Fax: +31-20-44 440844; E-mail: n.wolf@vumc.nl

**Funding Information**
The study received financial support from ZonMw TOP grant 91211005 (to S. H. K. and M. S. v. d. K.), the Optimix Foundation for Scientific Research (to M. S. v. d. K.), the ELA Foundation (ELA Grant 2009-045C3 and ELA Grant 2012-044PS5 to E. B.), the European Research Council (ERC Starting Grant 260888 to E. M. V.), the Fonds de Recherche du Québec en Santé (Research Scholar Junior 1 of FRQS) (to G. B.), the Fondation du Grand Defi Pierre Lavoie

## Abstract

**Objective**: The objective of this study was to investigate the genetic etiology of the X-linked disorder "Hypomyelination of Early Myelinating Structures" (HEMS). **Methods**: We included 16 patients from 10 families diagnosed with HEMS by brain MRI criteria. Exome sequencing was used to search for causal mutations. In silico analysis of effects of the mutations on splicing and RNA folding was performed. In vitro gene splicing was examined in RNA from patients' fibroblasts and an immortalized immature oligodendrocyte cell line after transfection with mutant minigene splicing constructs. **Results**: All patients had unusual hemizygous mutations of *PLP1* located in exon 3B (one deletion, one missense and two silent), which is spliced out in isoform DM20, or in intron 3 (five mutations). The deletion led to truncation of PLP1, but not DM20. Four mutations were predicted to affect *PLP1*/*DM20* alternative splicing by creating exonic splicing silencer motifs or new splice donor sites or by affecting the local RNA structure of the *PLP1* splice donor site. Four deep intronic mutations were predicted to destabilize a long-distance interaction

(grants to G. B.), the Canadian Institutes of Health Research (#301221 grant to C. D. M. v. K.), the Michael Smith Foundation for Health Research Scholar award (to C. D. M. v. K.), the National Institutes of Health (P20GM103464 and R01NS058978 to G. M. H.), the Kylan Hunter Foundation and the PMD Foundation (to G. M. H.).

Received: 14 January 2015; Revised: 3 March 2015; Accepted: 12 March 2015

***Annals of Clinical and Translational Neurology*** **2015; 2(6): 648–661**

doi: 10.1002/acn3.203

[a]These authors share first authorship.
[b]These authors share senior authorship.

structure in the secondary *PLP1* RNA fragment involved in regulating *PLP1*/*DM20* alternative splicing. Splicing studies in fibroblasts and transfected cells confirmed a decreased *PLP1*/*DM20* ratio. **Interpretation:** Brain structures that normally myelinate early are poorly myelinated in HEMS, while they are the best myelinated structures in Pelizaeus–Merzbacher disease, also caused by *PLP1* alterations. Our data extend the phenotypic spectrum of *PLP1*-related disorders indicating that normal *PLP1*/*DM20* alternative splicing is essential for early myelination and support the need to include intron 3 in diagnostic sequencing.

## Introduction

Among the childhood leukodystrophies, hypomyelinating disorders constitute a large, highly heterogeneous group of patients, many of whom remain without a genetically confirmed diagnosis.[1–4] Using magnetic resonance imaging (MRI) pattern recognition analysis, we previously identified a novel hypomyelinating disorder in four male patients in which hypomyelination is specifically pronounced in early myelinating structures.[1] As this distribution of hypomyelination is different from other hypomyelinating disorders, in which these early myelinating structures as a rule contain more myelin than the later myelinating structures,[4,5] we proposed a new disease called "Hypomyelination of Early Myelinating Structures" (HEMS).[1] Family history suggested X-linked inheritance, supported by the report of two brothers with the same clinical picture and MRI pattern.[1,6] The clinical phenotype of HEMS patients resembled that of other well-known hypomyelinating disorders, with onset of symptoms in late infancy, including ataxia and increasing spasticity, and relatively preserved cognition.[1,4,7–9] We hypothesized that HEMS could be caused by mutations of an X-chromosomal gene involved in the regulation of early myelination.[1,6] Diagnostic Sanger sequencing for known causes of hypomyelination, including Pelizaeus–Merzbacher disease (PMD), caused by X-linked *PLP1* mutations, and Pelizaeus–Merzbacher-like disease (PMLD), caused by *GJC2* mutations, had been unrevealing.[1]

The combination of MRI pattern recognition analysis, which is used for the categorization of homogeneous groups of patients with an unclassified white matter disorder and exome sequencing has been shown to be successful in identifying novel disease genes and new phenotypes associated with known disease genes.[10–12] In this study, we used the same approach and ascertained mutations in a specific region of *PLP1* that had initially not been identified. *PLP1* is located on the X-chromosome, contains seven exons and encodes both proteolipid protein 1 (PLP1) and its smaller isoform DM20 that is derived by the use of an alternative splice donor site within exon 3.[13] In all HEMS patients, the *PLP1* mutations are located either in the PLP1-specific region encoded by exon 3B that is spliced out in DM20 or in intron 3. Using in silico splicing prediction programs, in silico analysis of predicted secondary RNA structures, and in vitro analysis of gene splicing in RNA prepared from patients' fibroblasts and transfection studies, we show that these mutations play a role in alternative splicing of *PLP1*.

## Patients and Methods

### MRI studies and clinical examination

We included 16 male patients from 10 unrelated families (Table 1). Thirteen of the 16 patients were included based on their specific MRI pattern compatible with HEMS.[1] Seven of these 13 patients were identified from our MRI-database of over 3000 cases with an unclassified leukoencephalopathy using MRI pattern recognition analysis,[3] and six patients were previously identified and described (patients 8, 9, 11, and 12,[1] and patients 4 and 10[6]). S. H. K. and N. I. W. evaluated the MRIs according to a published protocol.[3] Three affected male siblings (patients 5, 15, and 16) were included without MR images. Clinical and laboratory investigations were retrospectively reviewed. Diagnostic Sanger sequencing of *PLP1* in patients 1, 2, 3, 8, 9, 11, 12, and 14 had previously been performed in diverse laboratories and reported unrevealing.

 

**Table 1.** *PLP1* mutations, in silico predictions and *PLP1/DM20* ratio.

| | | | | | In silico predictions | | | | | | In vitro studies | |
|---|---|---|---|---|---|---|---|---|---|---|---|---|
| | | | | | Missense prediction | Splicing effects | | | Mfold analysis | | *PLP1/DM20* ratio of normal | |
| Patients | c.DNA | Protein | Mother carrier | Nuc. conservation[1] | SIFT/poly-phen2/ mutation Taster | Predicted new splice sites[2] | Predicted change in strength natural *PLP1* splice donor site[2] | Predicted change number ESE[3]/ESS[4] motifs | LDIS-5′ & LDIS-3′ normal [ΔG]-mutant [ΔG][5] | Predicted conformational changes *PLP1* splice donor site exon 3B | Transfection study | Patients' fibroblasts |
| 1 | c.380_ 392del | p.(Arg127Lysfs* 16) | Yes | 1 | n.a. | n.d. | n.d. | n.d. | n.d. | n.d. | n.d. | n.d. |
| 4[6,7],10[6,7] | c.404T>G | p.(Leu135Trp) | Yes | 1 | D/B/B | No | No | +2 ESS | n.d. | Yes | n.d. | n.d. |
| 13[7], 14[7] | c.436C>T | p.= | Yes | 1 | n.a. | Yes[8] | No | +2 ESS | n.d. | No | 0.18 | n.d. |
| 8[9] | c.441A>T | p.= | No | 1 | n.a. | Inconclusive[10] | No | +1 ESS | n.d. | Yes | 0.14 | 0.01 |
| 6 | c.453+ 7A>G | p.? | n.d. | 1 | n.a. | Inconclusive[11] | Inconclusive[12] | +1 ESE (sc35) | n.d. | Yes | 0.05 | 0.06 |
| 2[13],3[13],5[7], 11[9,7] 15[13],16[13] | c.453+ 159G>A | p.? | 2,3,15,16 n.d.; 5&11 yes | 1 | n.a. | No | No | No | +5.1 | n.d. | n.d. | n.d. |
| 7 | c.453+ 164G>A | p.? | No | 1 | n.a. | Inconclusive[14] | No | Change strength ESE (sc35) | +5.9 | n.d. | n.d. | n.d. |
| 9[9] | c.454– 312C>G | p.? | Yes | 1 | n.a. | No | No | +3 ESS, + 1 ESE (sc35) | +4.1 | n.d. | n.d. | n.d. |
| 12[9] | c.454– 314T>G | p.? | No | 1 | n.a. | No | No | No | +1.6 | n.d. | 0.12[15] | n.d. |

For a detailed description of methods and programs used see Data S1. c.DNA, complementary DNA; nuc., nucleotide; n.a., not applicable; n.d., not done; B, benign; D, damaging; LDIS-5′, long-distance interaction site 5′; LDIS-3′, long-distance interaction site 3′; SC35, serine/arginine-rich splicing factor 2.

[1]Assessed using Phastcons scores (0 = no conservation, 1 = high conservation).

[2]Predicted new splice donor or acceptor sites. Yes = significant change, inconclusive = inconclusive change.

[3]Predicted change in number exonic splicing enhancers (ESE) motifs identified by ESE Finder 3.0.

[4]Predicted change in number exonic splicing silencer (ESS) motifs identified by FAS-ESS web server using the FAS-hex2 set.

[5]Difference of [ΔG] = minimal Gibbs energy, free energy, kcal/mole of the intra-intronic RNA structure fragment between the normal and mutant. Normal [ΔG] = −17.6 kcal/mole.

[6]Patients previously published by Tonduti et al.[6]

[7]Sibling pairs are as follows: 4 and 10, 5 and 11, and 13 and 14.

[8]Predicted strength of new splice donor site at c.434 of 87 by Human splice site finder (HSF) (normal range 0–100), 0.8 by NNsplice (normal range 0–1), 76.3 by Splice Site Finder (normal range 0–100), 0.8 confidence by Netgene2 (normal confidence range 0–1) and 3.4 by MaxEnt (normal range 0–12).

[9]Patients previously published by Steenweg et al.[1]

[10]Predicted strength of new splice donor site at c.439 of 79, by HSF (normal range 0–100).

[11]Predicted increase in potential acceptor splice site at c.453+15 strength of 45.7% (2.6–3.8) by MaxEnt (normal rang 0–16).

[12]Predicted decrease of 21% (0.7–0.5) by NNsplice (normal range 0–1).

[13]Patients belong to the same family.

[14]Predicted strength new splice donor site at c.453+161 of 2.3 by MaxEnt (normal range 0–12).

[15]Previously investigated and reported by us.[23]

## Informed consent

We received approval of the ethical standards committee for our gene identification research on patients with unclassified leukoencephalopathies at the VU University Medical Center in Amsterdam. All guardians of the patients participating in this study gave written informed consent. Approval was also obtained from the Institutional Review Board at Nemours/Alfred I. duPont Hospital for Children and the BC Children's Hospital, University of British Columbia, Canada, and informed consent was obtained as appropriate on the patients studied at these institutions.

## Whole-exome sequencing

Whole-exome sequencing (WES) on DNA from patients 5 and 11 (brothers), their mother, and patient 9, was performed using SeqCap EZ Human Library v3.0 kit (Nimblegen, Madison, WI, US) on a HiSeq2000 (Illumina, San Diego, CA). Coverage of at least 20× was reached for >96% of the targeted regions. Average sequencing depth ranged between 58 and 71. Data analysis was performed as described previously.[14] For three families, WES had been initiated in three other institutes, and available WES data were used for identification of mutations after recognition of the gene.

## Targeted sequencing of the X-chromosome exome

X-chromosome exome sequencing on DNA from patients 4 and 10 (brothers), 5 and 11 (brothers), 8 (including parents), 9 and 12 (including parents), was performed using SureSelectXT X-chromosome kit (Agilent, Santa Clara, CA, US) on a HiSeq2000 (Illumina, San Diego, CA). For all samples, coverage of at least 30× was reached for >80% of the targeted regions. Average sequencing depth ranged between 335 and 645. Data analysis was performed as described previously.[15]

## Validation and detection of *PLP1* variants

Validation and segregation of the identified *PLP1* variants in patients 1, 4, 5, and 7–12 by exome sequencing analysis was performed using standard Sanger sequencing. Primers were designed (Primer 3 V.0.4.0)[16,17] using reference sequence: *PLP1,* NM_000533.3. In patient 6, all 7 exons and intron–exon boundaries of *PLP1* were sequenced; in the remaining patients, only exon 3 and intron 3 of *PLP1* were sequenced using suitable primers (available upon request).

## In silico analysis of effects of the identified variants

Pathogenicity of missense variants was predicted using SIFT,[18] PolyPhen-2[19] and Mutation Taster.[20] Conservation of nucleotides was analyzed using Phastcons scores, obtained via Alamut version 2.4.

## In silico splicing analysis

The predicted effects of identified variants in *PLP1* on splicing were analyzed using different programs (details see in Data S1). A deviation of ≥10% from the normal score was considered as a change likely to affect splicing if present in at least three splice site prediction tools[21] (indicated by "yes" in Table 1). A deviation of ≥10% from the normal score in less than 3 splice site predictions tools was considered an inconclusive result. Changes of <10% were regarded as not significant and not reported. Predicted changes of number of exonic splice enhancer and silencer motifs were determined using default threshold values.

## In silico analysis of secondary *PLP1* RNA folding

The mfold program accessed via their web server with standard parameters was used to analyze *PLP1* normal and mutant RNA sequences for changes in the secondary pre-mRNA structure and stability (http://mfold.rna.albany.edu/?q=mfold/RNA-Folding-Form).[22] Using mfold, the four intronic mutations c.453+159G>A, c.453+164G>A, c.454−312C>G, and c.454−314T>G were analyzed using mutant RNA sequences including two regions within intron 3 of *PLP1*: 20 bases from c.453+150 to +169 and 20 bases from c.454−326 to −307, separated by 15 random bases ($N_{15}$), as previously described by us.[23] The four mutations c.404T>G, c.436C>T, c.441A>T, and c.453+7A>G were analyzed using mutant *PLP1* RNA sequences comprising exon 3 (c.192−c.453) and 40 flanking intronic nucleotides. As a measurement for the splice donor site accessibility by the spliceosome, conformational changes of the *PLP1* splice donor site in exon 3B and the *DM20* splice donor site in exon 3A, were visually examined and quantified by counting the nucleotides of the consensus *PLP1* splice donor site (c.451 to c.453+6: AAGGUGAUC) that were predicted to form base pairs.

## *PLP1/DM20* alternative splicing studies

### Minigene splicing construct transfection assay

The effects of three *PLP1* mutations c.436C>T, c.441A>T, and c.453+7G>A on *PLP1/DM20* alternative splicing were

 

individually investigated in a minigene splicing reporter construct transfection assay using Oli-neu cells, an immortalized cell line representing immature oligodendrocytes, as previously described, with modified reverse transcription (RT) (details in Data S1).[23,24]

### Skin fibroblast cultures

*PLP1/DM20* alternative splicing was investigated in skin fibroblasts from patient 6 harboring the c.453+7A>G intronic mutation. In addition, skin fibroblasts were available from a patient described in 1991 with the c.441A>T silent mutation,[25] the same as identified in patient 8 from our HEMS cohort. RT-PCR analysis of RNA prepared from cultured skin fibroblasts was performed as previously described with modified RT reaction (details in Data S1).[23]

## Results

### MRI findings

Detailed MRI findings of all patients in our cohort except three affected siblings are provided in Table S1 and Figures 1, 2. These patients had the characteristic MRI features corresponding to the previously described disorder "HEMS".[1] On initial MRIs, patients had mild $T_2$ hyperintensity of the medulla oblongata, the pons, especially at the border with the medulla oblongata, and the hilus of the dentate nucleus, with variable $T_2$ hyperintensity of the peridentate white matter, indicating hypomyelination of these regions (Figs. 1A and B, 2I and J). Mild $T_2$ hyperintensity of the optic radiation, periventricular white matter and parietal white matter was observed in all patients (Figs. 1C, 2K), with extensions into the subcortical white matter under the pericentral cortex in eight patients (Figs. 1D, 2L). Patients 1 and 6 had more extensive subcortical white matter hypomyelination. All patients had alternating $T_2$ hyperintense–hypointense–hyperintense stripes in the posterior limb of the internal capsule (Figs. 1C, 2K). The thalamus had a mildly elevated $T_2$ signal, except for its ventrolateral part, which was darker, a configuration that is normally seen in neonates (Figs. 1C, 2K). On follow-up, the $T_2$ signal abnormalities of the medulla oblongata and pons improved in four of the eight patients in whom repeat images were available, indicating progressing myelination (Fig. 1I and J). The periventricular and deep white matter and/or corpus callosum showed more extensive $T_2$ hyperintensity than before in seven of the eight patients, indicating myelin loss (Fig. 1K and L). After identification of mutations in the gene *PLP1* (see below), two clinically asymptomatic female carriers (c.454−312C>G, age 40 years, and c.453+159G>A, age 53 years) underwent brain MRI, which demonstrated mild global atrophy of the cerebral hemispheres and diffuse mild $T_2$ hyperintensity of the supratentorial white matter (data not shown).

### Clinical profiles and laboratory results

Detailed clinical characteristics are provided in Table S2. Twelve of the 16 patients presented with nystagmus in the first or second year of life. The other four patients presented first with cerebellar dysfunction or developmental delay. All patients continued to gain motor skills, but mostly delayed. All developed progressive spasticity of the legs and signs of cerebellar dysfunction. At last clinical follow-up, five patients (age range 3–12 years) could still walk without support, although they had an evident spastic-ataxic gait. Five patients used braces or a walker for ambulation, and five needed a wheelchair. One was still too young to judge his ability to walk. Cognitive capabilities were normal or mildly impaired. All female carriers were clinically normal. Nerve conduction studies performed in eight patients revealed normal motor and sensory conduction velocities in all except patient 1 who had delayed conduction velocities in his legs.

### Genetic analysis

We first performed WES in two brothers and their mother and an unrelated patient. Under the hypothesis of an X-linked recessive inheritance model, we selected all rare hemizygous variants (variants with a minor allele frequency of ≤1% in known public control databases; 1000 Genomes, dbSNP137 and National Heart, Lung, and Blood Institute Exome Sequencing Project (http://evs.gs.washington.edu/EVS/), and absence from our in-house control samples), located on the X-chromosome. With this approach we were unable to identify a candidate gene. We subsequently performed targeted sequencing of the X-chromosome exome including four additional HEMS patients and parents. The same filtering strategy was used, and genes were selected if variants were present in at least two unrelated patients. This led us to the identification of one candidate gene: *PLP1* (MIM 300401), encoding PLP1 (shown in Fig. 3A). Two exonic variants were identified: a c.404T>G missense variant, predicting p.(Leu135Trp) and a c.441A>T silent variant. Manual analysis of the intron data revealed three variants located deep in intron 3. Coverage of two of these variants, c.454−312C>G and c.454−314T>G, was very poor for both the WES and the X-chromosome exome approach (<5 reads), while the c.453+159G>A variant was sufficiently covered with the X-chromosome exome (63–97 reads) (data not shown). In the nine remaining HEMS patients *PLP1* variants were identified either by Sanger

 

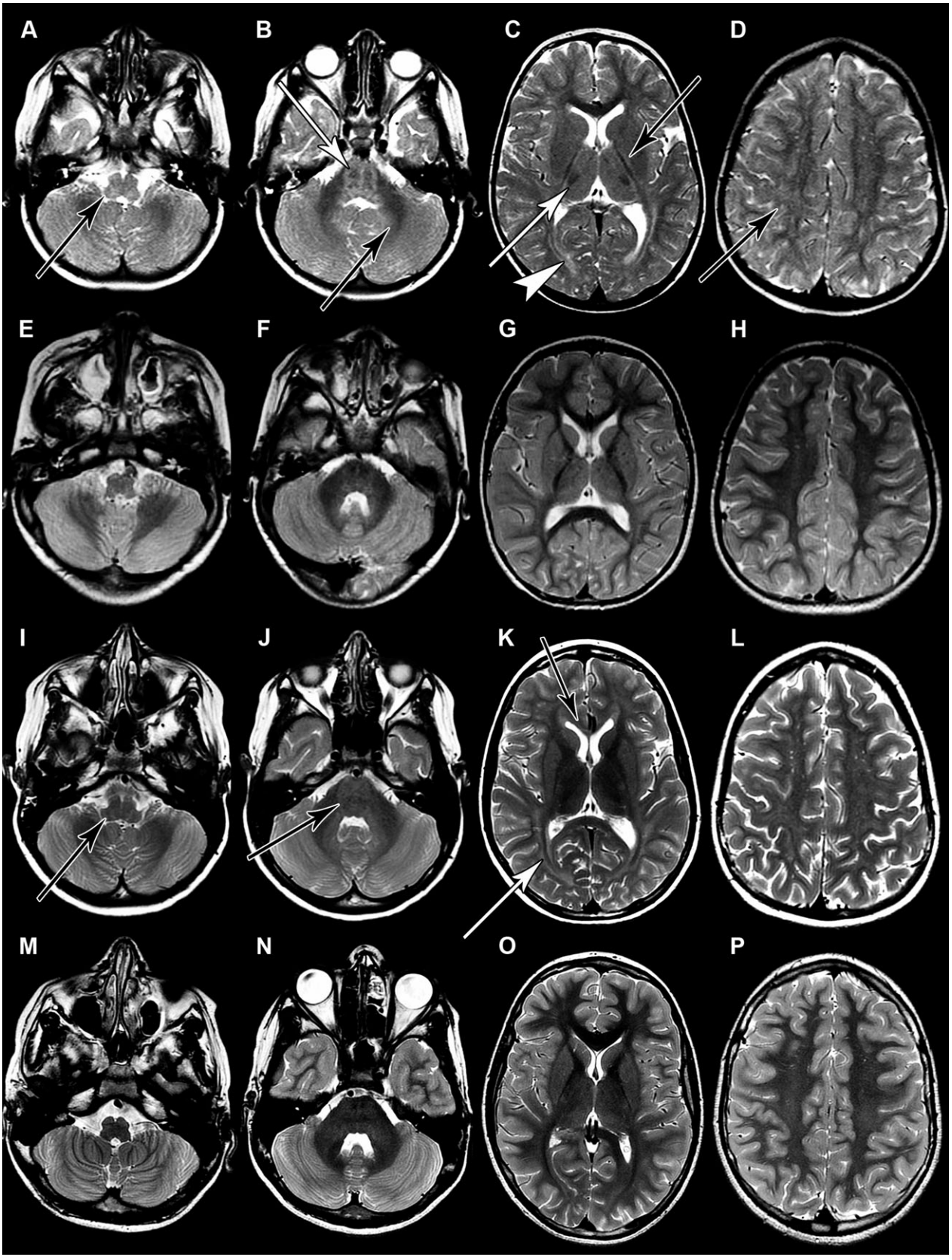


 

**Figure 1.** MRI of HEMS patients. Initial MRIs of patient 9 (A–D, age 3 years), and of an age-matched control (E–H, 2.5 years) and follow-up MRIs of patient 9 (I–L, age 12.4 years), and of an age-matched control (M–P, 12 years). All images are axial $T_2$-weighted. MRIs of patient 9 show mild $T_2$ hyperintensity of the medulla oblongata (A, arrow), the pons (B, white arrow) and the hilus of the dentate nucleus (B, black arrow). The thalamus is mildly $T_2$ hyperintense, except for its ventrolateral part, which is dark (C, white arrow). The posterior limb of the internal capsule shows alternating hyperintense–hypointense–hyperintense stripes (C, black arrow). There is mild $T_2$ hyperintensity of the optic radiation (C, white arrowhead) and the periventricular white matter that extends into the central subcortical white matter (D, black arrow). At later stages, the $T_2$ signal in the medulla and pons improves (I and J), but the $T_2$ hyperintensity of the optic radiation (K, white arrow), the corpus callosum (K, black arrow) and the periventricular white matter and subcortical white matter increases. Control images (E–H and M–P) show the normal myelination pattern with respect to age.

sequencing or by WES data retrieved from other institutes. In total, nine different *PLP1* variants were identified in 16 patients (10 families) (Table 1, Fig. 3B). All variants were located in exon 3B or intron 3 (Fig. 3A and B). The mutations were maternally inherited in five families and de novo in three families. In two families, the mother was not available for testing. However, multiple affected family members indicated obligate carriership.

## In silico analyses of effects of the identified *PLP1* variants

The c.380_392del variant was predicted to result in a frameshift p.(Arg127Lysfs*16) truncating PLP1, but not DM20. For the other eight identified *PLP1* variants, we performed several in silico bioinformatics prediction analyses to investigate pathogenicity. An overview of the results is depicted in Table 1.

## In silico splicing analysis

Of the eight variants, only the silent c.436C>T change was predicted to have an effect on splice sites by creating a new splice donor site in exon 3B at position c.434. Analysis of splice regulatory elements showed that for all three exonic variants and the c.454−312C>G variant 1–3 new exonic splicing silencer motifs were predicted.

## In silico analysis of secondary *PLP1* RNA folding

Using mfold, we previously found that two regions within intron 3 of *PLP1* form an intramolecular base-pairing interaction in the predicted secondary *PLP1* RNA structure and play an important role in the control of *PLP1*/*DM20* alternative splicing.[23] In our HEMS cohort, we found four variants in either of these two regions (Fig. 3B and C). The 5′ region (c.453+151 to c.453+166) is referred to as the long-distance interaction (LDI) site 5′ (LDIS-5′) and the 3′ region (c.454−323 to c.454−308) as the LDIS-3′ (Fig. 3C). Mutations created in LDIS-5′ and LDIS-3′ sequences that were predicted to destabilize this secondary *PLP1* RNA structure (initial Gibbs free energy [ΔG] value less than −16.4 kcal/mole) decreased the ratio of alternatively spliced products *PLP1* to *DM20* in a minigene reporter system, while mutations of the central nonpairing bases, c.453+158 and c.454−315, and mutations that were predicted to maintain the secondary structure did not.[23] We investigated the effect of the four variants identified in our families, two in LDIS-5′ (c.453+159G>A and c.453+164G>A) and two in LDIS-3′ (c.454−312C>G and c.454−314T>G), on the LDI structure and found that in all cases the stability of the mutant LDI structures was predicted to be reduced ([ΔG] values of less than −16.4 kcal/mole) compared with the normal fragment ([ΔG of −17.6 kcal/mole]) (Fig. S1).

Analysis of the predicted secondary *PLP1* RNA structures for the remaining four variants c.404T>G, c.436C>T, c.441A>T, and c.453+7A>G showed that all except the c.436C>T variant increased the stability of the local RNA structure of the *PLP1* splice donor site, while leaving the structure of the *DM20* splice donor site unchanged (Table S3). These predictions suggest that the *PLP1* splice donor site is more engaged in intramolecular base pairing in the mutated RNA fragments than in the normal RNA fragments.

## *PLP1*/*DM20* alternative splicing studies in a minigene splicing construct assay

In a reporter construct transfection assay,[23,24] we investigated the effects of the c.436C>T, the c.441A>T, and the c.453+7A>G mutation on *PLP1/DM20* alternative splicing. These mutations resulted in a significant reduction in the *PLP1*/*DM20* ratio to 0.18 (c.436C>T), 0.14 (c.441A>T), and 0.05 (c.453+7A>G) of normal (Fig. 4A). We could not detect the potentially aberrantly spliced product from the new splice donor site predicted for the c.436C>T mutation. The effect of the c.454−314T>G mutation was previously reported by us and resulted in a *PLP1/DM20* ratio of 0.15 of normal.[23]

## *PLP1*/*DM20* alternative splicing studies in fibroblasts

In patient fibroblasts, we investigated the effect of the c.441A>T and the c.453+7A>G mutation on the *PLP1*/*DM20* ratio and found it reduced to 0.01 and 0.06 of normal (Fig. 4B). We consider this to be a rough estimate

 

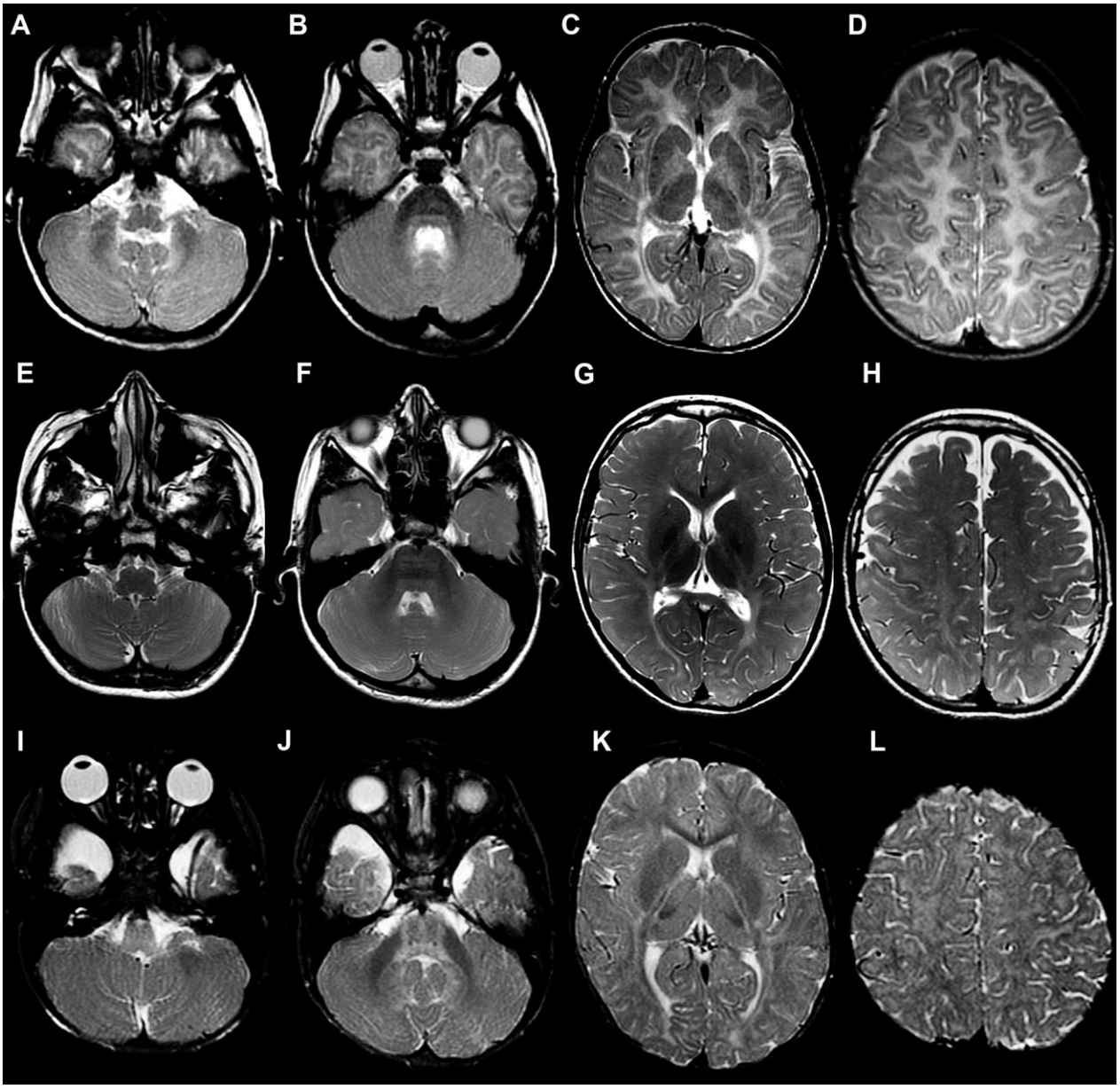


**Figure 2.** MRI of *PLP1*-related disorders. MRI of a patient with: classic Pelizaeus–Merzbacher disease (PMD) harboring a *PLP1* duplication (A–D, age 23 months), Spastic Paraplegia type 2 (SPG2) with a frameshift mutation (c.263delC, p.(Ala88Valfs*26)) (E–H, age 11.4 years) and patient 11 with hypomyelination of early myelinating structures (HEMS) harboring an intronic mutation (c.453+159G>A) (I–L, age 20 months). All MR images are axial $T_2$-weighted. Note that in the patients with PMD (A and B) and SPG2 (E and F), the medulla oblongata and the pons show a normal dark $T_2$ signal, in contrast to the patient with HEMS (I and J), in whom these structures are mildly $T_2$ hyperintense. The alternating hyperintense–hypointense–hyperintense stripes in the posterior limb of the internal capsule seen commonly in HEMS patients (K) are not present in the patient with PMD (C) or SPG2 (G). All the three illustrated patients have $T_2$ hyperintensity of the periventricular white matter, deep white matter and subcortical white matter, which is diffuse and extensive in the patient with PMD (C and D), restricted in the patient with SPG2 (G and H), and intermediate in the patient with HEMS (K and L).

of the reduction in *PLP1/DM20* ratio because there is very little *PLP1* compared with *DM20* in skin fibroblasts and we noted that the amount of total *PLP1* (*PLP1* + *DM20*) decreases with passage number.

## Discussion

Using exome sequencing, we identified the genetic defect causing HEMS.[1] All patients had hemizygous mutations

 

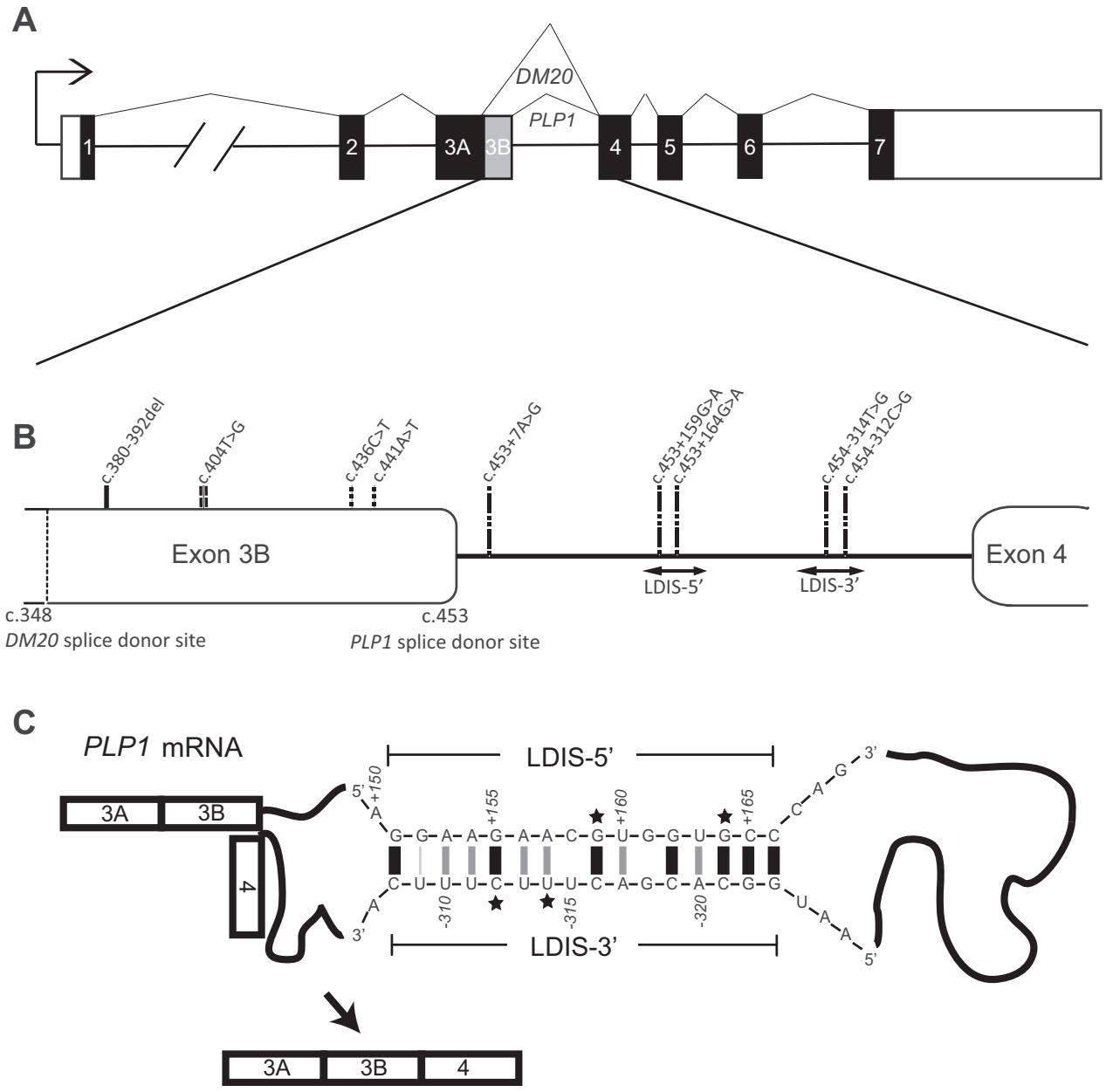


**Figure 3.** Overview of *PLP1* mutations and predicted secondary *PLP1* RNA structure. This overview illustrates *PLP1* gene structure with its seven exons (black boxes) and the two alternative transcripts, *PLP1* or *DM20*, resulting from a splice donor site within exon 3 (A). Close-up of exon 3B and intron 3 is depicted in (B). All nine mutations found in our hypomyelination of early myelinating structures (HEMS) cohort are shown. The frameshift mutation is indicated with a black solid line, the two silent mutations with a dashed line and the single missense mutation with two striped lines. Intronic mutations are indicated with an interrupted line. The secondary *PLP1* RNA structure is displayed in (C), illustrating the formation of the predicted long-distance interaction (LDI) structure between LDIS-5′ and LDIS-3′ within intron 3. Mutated positions in our HEMS cohort are indicated with stars. Adapted from Taube et al.[23] with permission of Oxford University press.

in the *PLP1* gene, which encodes both PLP1 and its smaller isoform DM20 that is derived by the use of an alternative splice donor site within exon 3.[13] Together the proteins constitute more than half of the total protein mass of myelin in the central nervous system (CNS).[26] The *DM20* transcript is preferentially expressed in the developing CNS before initiation of myelination, whereas the *PLP1* transcript dominates during myelination and adulthood, suggesting tightly regulated *PLP1/DM20* alternative splicing.

 

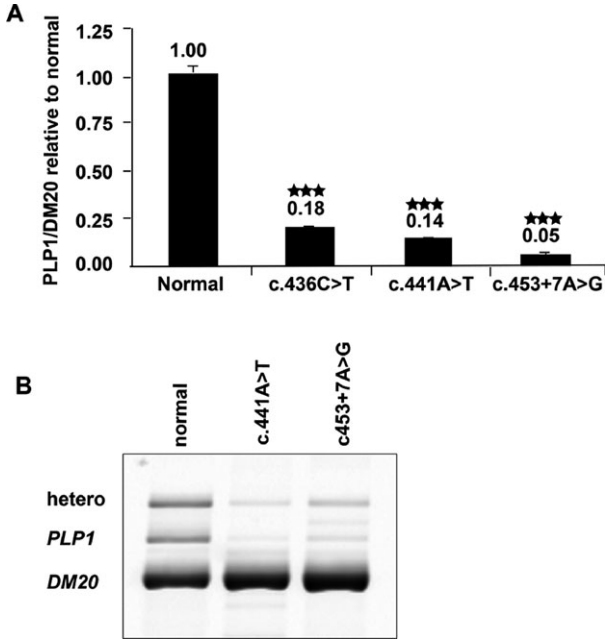


**Figure 4.** Dysregulation of *PLP1* splicing by patients' mutations. Quantitation of *PLP1/DM20* mRNA produced in an immature immortalized oligodendrocyte cell line from the transfected splicing minigene reporter construct indicated a significant decrease in the *PLP1/DM20* ratio with patients' mutations compared with normal construct (A). The graph shows the ratio of *PLP1* product to the *DM20* product from each patient construct normalized to the normal construct (mean of replicates ±SD). All constructs were tested in triplicate. All three patient constructs had a ratio significantly different from the normal construct, as measured by Student's *t*-test: ***, $P < 0.001$. Analysis of skin fibroblast RNA by RT-PCR indicated a decrease in *PLP1/DM20* ratio with patients' mutations (B). The primers that amplify from exon 2 to exon 5 *PLP1* readily detect *PLP1* and *DM20* signal in the same reaction as different sized bands. A heteroduplex of *PLP1* and *DM20* is also visible (*PLP1* and *DM20* heteroduplex formation has been described previously).[24] Quantitation performed by dividing *PLP1* + ½ heteroduplex band by *DM20* and normalizing, indicated *PLP1/DM20* ratio in patient fibroblasts was 0.01 of normal for c.441A>T and 0.06 of normal for c.453+7A>G. The *PLP1* band was 105 bases larger than the DM20 band.

*PLP1* mutations are known to be associated with a broad continuum of neurological phenotypes ranging from connatal PMD with severe hypomyelination to pure X-linked spastic paraplegia type 2 (SPG2) with even normal brain imaging in some cases.[5,7–9] Different genetic alterations have been identified to cause these different phenotypes, with duplication of the entire *PLP1* gene as the most common change usually leading to the classic form of PMD.[27] More severe forms are associated with missense mutations in highly conserved regions or, in rare cases, with triplications and higher copy number of *PLP1*, while patients with null mutations or missense mutations in less conserved regions present with milder signs.[28,29] Previously, we had defined HEMS based on the distinctive abnormalities seen on brain MRI. With the identification of *PLP1* mutations in this group, HEMS should be added as a recognizable new MRI phenotype within the broad spectrum of *PLP1*-related disorders.

Clinically, most patients with HEMS have a relatively mild functional disability and can be classified as complicated SPG2. All patients, except for patient 1 harboring the truncating *PLP1* mutation (p.(Arg127Lysfs*16)) have normal nerve conduction studies or sensory function on physical examination. This is in agreement with the hypothesis that only patients lacking PLP1 due to a functional null mutation or a truncating mutation in the PLP1-specific region have a peripheral neuropathy.[28,30–32] In five families, the mutation was inherited from the mother. All female carriers were clinically asymptomatic, but the two females who underwent MR imaging showed abnormalities consisting of mild atrophy of the cerebral hemispheres and a diffuse $T_2$ hyperintensity of the white matter. This phenomenon has also been observed in carriers of mutations associated with a mild PMD phenotype,[32,33] and can be explained by random X-inactivation due to the mild effects of these mutations.[8,9]

Remarkably, in our HEMS cohort, the identified *PLP1* mutations were restricted to the PLP1 specific region encoded by exon 3B that is spliced out in DM20, and to intron 3 (Fig. 3A and B). Only one family carried an obvious pathogenic *PLP1* mutation (p.(Arg127Lysfs*16)). The other nine families had presumed "subtle" *PLP1* mutations: these mutations were located in the noncoding region outside the splice donor and acceptor sites of exon 3B in six families; a silent mutation was identified in two families, and a missense mutation for which pathogenicity predictions were contradictory was identified in one family. This is in contrast to the commonly reported mutations in exon 3B that are mainly missense, truncating or located at the splice donor site sequence of exon 3B.[28,30–32,34–47]

We provide evidence that the mutations ascertained in our HEMS cohort alter *PLP1/DM20* alternative splicing and must therefore be interpreted as pathogenic. Splicing is a complex mechanism not only controlled by the canonical splice donor and acceptor sites and branch sites but also by exonic or intronic enhancers and silencers and by regulation through the secondary RNA structure.[23,24,42,45,48–51] We first performed in silico prediction analysis on the effects of the variants concerning these regulatory factors. Splice site predictions for the c.436C>T mutation showed a new *PLP1* splice donor site at c.434. For all three exonic substitutions (including c.436C>T) and for the intronic c.454−312C>G muta-

 

tion, the creation of putative new exonic silencer motifs was predicted. This mechanism had previously been found associated with loss of the *PLP1* isoform for a *PLP1* c.436C>G missense mutation.[52] Analysis of predicted secondary *PLP1* RNA structures containing the c.404T>G, c.441A>T and 453+7A>G mutations revealed potential conformational changes of the *PLP1* splice donor site that could result in a less accessible splice site for the spliceosome. This change may shift the balance between the usage of *DM20* and the *PLP1* exon 3 splice donor sites in disadvantage of the latter. Interestingly, the four noncoding mutations restricted to two specific regions deep within intron 3 of *PLP1* (LDIS-5′ and LDIS-3′) were predicted to reduce the stability of the secondary LDI *PLP1* RNA structure, which has been found associated with a decreased *PLP1* to *DM20* ratio.[23] Overall, these results indicate that the identified variants have an impact on *PLP1*/*DM20* alternative splicing. For the three tested variants (c.453+7A>G, c.436C>T, c.441A>T), we could confirm these predictions in vitro by detecting a decreased *PLP1*/*DM20* ratio in fibroblasts or in our minigene reporter transfection assay. Several additional algorithms applied for prediction of the impact of the single missense variant (c.404T>G) on protein structure and function showed contradictory results.

Although mutations in *PLP1* are also associated with PMD or SPG2, the MRI pattern of HEMS contrasts with the MRI findings in these disorders (see Fig. 2).[1,4,5] Normally, tracts become myelinated at the time they become functional, resulting in a fixed spatiotemporal sequence of myelination.[53] In patients with HEMS, the brain structures that normally myelinate early (e.g., brainstem, hilus of the dentate nucleus, posterior limb of the internal capsule, optic tracts and tracts to the pericentral cortex) are poorly myelinated in contrast to structures that normally myelinate at a later developmental stage, which show better myelination.[1,53] In patients with PMD and SPG2, however, the early myelinated structures are relatively better myelinated than other brain structures (Fig. 2A–H). This indicates that *PLP1/DM20* alternative splicing and maintenance of a certain PLP1 to DM20 ratio are important for early myelination.

Noteworthy, three mutations identified in our HEMS cohort have been reported before (c.436C>T,[34] c.441A>T,[25] and c.453+7A>G[46]). The patient with the c.436C>T had mild functional disability.[34] For the patients with the c.441A>T and c.453+7A>G mutation only the clinical diagnosis "PMD" was provided.[25,46] We recently also identified three PMD families with mutations in the LDIS-3′ region (including c.454−314T>G), with a mild clinical phenotype, comparable to HEMS patients.[23] No MRI data were available for these patients, so we were not able to evaluate whether these patients have an MRI phenotype compatible with HEMS.

Our HEMS cohort presents a challenge for *PLP1* Sanger sequencing in a diagnostic setting. For most mutations, pathogenicity was difficult to prove. For example, the two silent mutations, c.436C>T and c.441A>T, had already been identified in the past in our patients, but were thought to be benign. Moreover, the noncoding regions LDIS-5′ and LDIS-3′ in intron 3 are currently not included in *PLP1* diagnostic sequencing. Our data support the proposal that sequencing of intron 3 of *PLP1* should be included in standard diagnostic procedures because of the importance of this region for controlling *PLP1/DM20* alternative splicing.[23] Furthermore, this study illustrates that caution is warranted in case of negative exome sequencing results, as coverage is often not optimal for intronic regions. Thanks to the number of patients with identical clinical and MRI presentation, we were able to identify the genetic basis of HEMS. The identification of more patients with mutations in this or other regions of *PLP1* altering *PLP1*/*DM20* alternative splicing will further elucidate the specificity of the HEMS MRI phenotype within the PMD spectrum. Future research will show whether these mutations that affect *PLP1/DM20* alternative splicing could be potential targets for treatment aimed at correction of the PLP1 to DM20 ratio.

## Acknowledgments

We thank the families for their cooperation with our study, and all colleagues caring for the patients for their contributions. We are grateful to Dr. Chiara Aiello for sequencing candidate genes related to hypomyelination in some patients and to Dr. Marta Romani for her support with whole exome sequencing of Italian families. The study received financial support from ZonMw TOP grant 91211005 (to S. H. K. and M. S. v. d. K.), the Optimix Foundation for Scientific Research (to M. S. v. d. K.), the ELA Foundation (ELA Grant 2009-045C3 and ELA Grant 2012-044PS5 to E. B.), the European Research Council (ERC Starting Grant 260888 to E. M. V.), the Fonds de Recherche du Québec en Santé (Research Scholar Junior 1 of FRQS) (to G. B.), the Fondation du Grand Defi Pierre Lavoie (grants to G. B.), the Canadian Institutes of Health Research (#301221 grant to C. D. M. v. K.), the Michael Smith Foundation for Health Research Scholar award (to C. D. M. v. K.), the National Institutes of Health (P20GM103464 and R01NS058978 to G. M. H.), the Kylan Hunter Founda-

 

tion and the PMD Foundation (to G. M. H.). The content is solely the responsibility of the authors and does not necessarily represent the official views of the granting agencies and foundations.

## Author Contribution

S. H. K., J. R. T., M. S. v. d. K., G. M. H., and N. I. W., designed the study. S. H. K., J. R. T., R. M. L. v. S., K. S., E. M. V., L. T., M. T. G., C. G. M. v. B., Q. W., T. E. M. A., G. M. H., N. I. W., performed experiments, collected and analyzed data. E. B., M. T., D. T., E. A. S., G. B., C. E. C., C. D. M. v. K., J. R. Ø., R. L. F., M. F. E., J. H. S., S. O., M. E. S., M. S. v. d. K., G. M. H., N. I. W., provided patient data and collected samples. S. H. K., and N. I. W., wrote the manuscript. All authors read the manuscript and revised the manuscript for important intellectual content.

## Conflict of Interest

G. B.: grants and personal fees from Actelion Pharmaceuticals, personal fees from Genzyme, personal fees from Shire, grants from CIHR, grants from FRQS, grants from CIHR-Genome Canada, grants from Fondation Les Amis d'Eliott, grants from Fondation sur les Leucodystrophies, grants from Montreal Children's Hospital, and McGill University Health Center Research Institutes; outside the submitted work.

### References

1. Steenweg ME, Wolf NI, Schieving JH, et al. Novel hypomyelinating leukoencephalopathy affecting early myelinating structures. Arch Neurol 2012;69:125–128.
2. Steenweg ME, Vanderver A, Blaser S, et al. Magnetic resonance imaging pattern recognition in hypomyelinating disorders. Brain 2010;133:2971–2982.
3. van der Knaap MS, Breiter SN, Naidu S, et al. Defining and categorizing leukoencephalopathies of unknown origin: MR imaging approach. Radiology 1999;213: 121–133.
4. Pouwels PJ, Vanderver A, Bernard G, et al. Hypomyelinating leukodystrophies: translational research progress and prospects. Ann Neurol 2014;76:5–19.
5. van der Knaap MS, Valk J. Pelizaeus-Merzbacher disease and X-linked spastic paraplegia type 2. In Magnetic resonance of myelination and myelin disorders. 3rd ed. Berlin: Springer, 2005. p. 272–280.
6. Tonduti D, Pichiecchio A, Wolf NI, et al. Novel hypomyelinating leukoencephalopathy affecting early myelinating structures: clinical course in two brothers. Neuropediatrics 2013;44:213–217.
7. Woodward KJ. The molecular and cellular defects underlying Pelizaeus-Merzbacher disease. Expert Rev Mol Med 2008;10:e14.
8. Inoue K. PLP1-related inherited dysmyelinating disorders: Pelizaeus-Merzbacher disease and spastic paraplegia type 2. Neurogenetics 2005;6:1–16.
9. Hudson LD. Pelizaeus-Merzbacher disease and spastic paraplegia type 2: two faces of myelin loss from mutations in the same gene. J Child Neurol 2003;18:616–624.
10. Kevelam SH, Bugiani M, Salomons GS, et al. Exome sequencing reveals mutated SLC19A3 in patients with an early-infantile, lethal encephalopathy. Brain 2013;136:1534–1543.
11. Dallabona C, Diodato D, Kevelam SH, et al. Novel (ovario) leukodystrophy related to AARS2 mutations. Neurology 2014;82:2063–2071.
12. Taft RJ, Vanderver A, Leventer RJ, et al. Mutations in DARS cause hypomyelination with brain stem and spinal cord involvement and leg spasticity. Am J Hum Genet 2013;92:774–780.
13. Nave KA, Lai C, Bloom FE, et al. Splice site selection in the proteolipid protein (PLP) gene transcript and primary structure of the DM-20 protein of central nervous system myelin. Proc Natl Acad Sci USA 1987;84:5665–5669.
14. Wolf NI, Salomons GS, Rodenburg RJ, et al. Mutations in RARS cause hypomyelination. Ann Neurol 2014;76:134–139.
15. Ameziane N, Sie D, Dentro S, et al. Diagnosis of fanconi anemia: mutation analysis by next-generation sequencing. Anemia 2012;2012:132856.
16. Untergasser A, Cutcutache I, Koressaar T, et al. Primer3–new capabilities and interfaces. Nucleic Acids Res 2012;40: e115.
17. Koressaar T, Remm M. Enhancements and modifications of primer design program Primer3. Bioinformatics 2007;23:1289–1291.
18. Ng PC, Henikoff S. Predicting deleterious amino acid substitutions. Genome Res 2001;11:863–874.
19. Adzhubei I, Jordan DM, Sunyaev SR. Predicting functional effect of human missense mutations using PolyPhen-2. Curr Protoc Hum Genet 2013;Chapter 7:Unit7.20. doi: 10.1002/0471142905.hg0720s76:Unit7
20. Schwarz JM, Cooper DN, Schuelke M, et al. MutationTaster2: mutation prediction for the deep-sequencing age. Nat Methods 2014;11:361–362.
21. Wallis Y, Payne S, McAnulty C, et al. Practice guidelines for the evaluation of pathogenicity and the reporting of sequence variants in clinical molecular genetics. Available at: http://www.acgs.uk.com/media/774853/evaluation_and_reporting_of_sequence_variants_bpgs_june_2013_-_finalpdf.pdf. Accessed May, 2014.
22. Zuker M. Mfold web server for nucleic acid folding and hybridization prediction. Nucleic Acids Res 2003;31:3406–3415.

 

23. Taube JR, Sperle K, Banser L, et al. PMD patient mutations reveal a long-distance intronic interaction that regulates PLP1/DM20 alternative splicing. Hum Mol Genet 2014;23:5464–5478.
24. Hobson GM, Huang Z, Sperle K, et al. A PLP splicing abnormality is associated with an unusual presentation of PMD. Ann Neurol 2002;52:477–488.
25. Pratt VM, Dlouhy SR, Hodes ME. Possible cryptic splice site found in the PLP gene in a patient with Pelizaeus-Merzbacher disease. Am J Hum Genet 1991;49 (suppl):393–451.
26. Eng LF, Chao FC, Gerstl B, et al. The maturation of human white matter myelin. Fractionation of the myelin membrane proteins. Biochemistry 1968;7:4455–4465.
27. Sistermans EA, de Coo RF, De Wijs IJ, et al. Duplication of the proteolipid protein gene is the major cause of Pelizaeus-Merzbacher disease. Neurology 1998;50:1749–1754.
28. Cailloux F, Gauthier-Barichard F, Mimault C, et al. Genotype-phenotype correlation in inherited brain myelination defects due to proteolipid protein gene mutations. Clinical European Network on Brain Dysmyelinating Disease. Eur J Hum Genet 2000;8:837–845.
29. Wolf NI, Sistermans EA, Cundall M, et al. Three or more copies of the proteolipid protein gene PLP1 cause severe Pelizaeus-Merzbacher disease. Brain 2005;128:743–751.
30. Shy ME, Hobson G, Jain M, et al. Schwann cell expression of PLP1 but not DM20 is necessary to prevent neuropathy. Ann Neurol 2003;53:354–365.
31. Osaka H, Kawanishi C, Inoue K, et al. Novel nonsense proteolipid protein gene mutation as a cause of X-linked spastic paraplegia in twin males. Biochem Biophys Res Commun 1995;215:835–841.
32. Hodes ME, Blank CA, Pratt VM, et al. Nonsense mutation in exon 3 of the proteolipid protein gene (PLP) in a family with an unusual form of Pelizaeus-Merzbacher disease. Am J Med Genet 1997;69:121–125.
33. Nance MA, Boyadjiev S, Pratt VM, et al. Adult-onset neurodegenerative disorder due to proteolipid protein gene mutation in the mother of a man with Pelizaeus-Merzbacher disease. Neurology 1996;47:1333–1335.
34. Laukka JJ, Stanley JA, Garbern JY, et al. Neuroradiologic correlates of clinical disability and progression in the X-linked leukodystrophy Pelizaeus-Merzbacher disease. J Neurol Sci 2013;335:75–81.
35. Saugier-Veber P, Munnich A, Bonneau D, et al. X-linked spastic paraplegia and Pelizaeus-Merzbacher disease are allelic disorders at the proteolipid protein locus. Nat Genet 1994;6:257–262.
36. Sivakumar K, Sambuughin N, Selenge B, et al. Novel exon 3B proteolipid protein gene mutation causing late-onset spastic paraplegia type 2 with variable penetrance in female family members. Ann Neurol 1999;45:680–683.
37. Gorman MP, Golomb MR, Walsh LE, et al. Steroid-responsive neurologic relapses in a child with a proteolipid protein-1 mutation. Neurology 2007;68:1305–1307.
38. Grossi S, Regis S, Biancheri R, et al. Molecular genetic analysis of the *PLP1* gene in 38 families with PLP1-related disorders: identification and functional characterization of 11 novel PLP1 mutations. Orphanet J Rare Dis 2011;6:40–46.
39. Osaka H, Koizume S, Aoyama H, et al. Mild phenotype in Pelizaeus-Merzbacher disease caused by a PLP1-specific mutation. Brain Dev 2010;32:703–707.
40. Pratt VM, Trofatter JA, Larsen MB, et al. New variant in exon 3 of the proteolipid protein (PLP) gene in a family with Pelizaeus-Merzbacher disease. Am J Med Genet 1992;43:642–646.
41. Pretorius E, Naude H, Ribbens C, et al. Pelizaeus-Merzbacher disease: a developmental disorder affecting myelin formation in the nervous system. J Dev Phys Disabil 2005;17:173–183.
42. Hobson GM, Huang Z, Sperle K, et al. Splice-site contribution in alternative splicing of PLP1 and DM20: molecular studies in oligodendrocytes. Hum Mutat 2006;27:69–77.
43. Pratt VM, Naidu S, Dlouhy SR, et al. A novel mutation in exon 3 of the proteolipid protein gene in Pelizaeus-Merzbacher disease. Neurology 1995;45:394–395.
44. Lassuthova P, Zaliova M, Inoue K, et al. Three new PLP1 splicing mutations demonstrate pathogenic and phenotypic diversity of Pelizaeus-Merzbacher disease. J Child Neurol 2014;29:924–931.
45. Hobson GM, Davis AP, Stowell NC, et al. Mutations in noncoding regions of the proteolipid protein gene in Pelizaeus-Merzbacher disease. Neurology 2000;55:1089–1096.
46. Hubner CA, Orth U, Senning A, et al. Seventeen novel PLP1 mutations in patients with Pelizaeus-Merzbacher disease. Hum Mutat 2005;25:321–322.
47. Bridge PJ, Wilkens PJ. The role of proteolipid protein gene in Pelizaeus-Merzbacher disease. Am J Hum Genet 1992;51 (suppl):A209.
48. Bonnet-Dupeyron MN, Combes P, Santander P, et al. PLP1 splicing abnormalities identified in Pelizaeus-Merzbacher disease and SPG2 fibroblasts are associated with different types of mutations. Hum Mutat 2008;29:1028–1036.
49. Wang E, Huang Z, Hobson GM, et al. PLP1 alternative splicing in differentiating oligodendrocytes: characterization of an exonic splicing enhancer. J Cell Biochem 2006;97:999–1016.
50. Wang E, Dimova N, Cambi F. PLP/DM20 ratio is regulated by hnRNPH and F and a novel G-rich

 

enhancer in oligodendrocytes. Nucleic Acids Res 2007;35:4164–4178.
51. Warf MB, Berglund JA. Role of RNA structure in regulating pre-mRNA splicing. Trends Biochem Sci 2010;35:169–178.
52. Regis S, Corsolini F, Grossi S, et al. Restoration of the normal splicing pattern of the *PLP1* gene by means of an antisense oligonucleotide directed against an exonic mutation. PLoS One 2013;8:e73633.
53. van der Knaap MS, Valk J. Myelination and retarded myelination. In: Magnetic resonance of myelination and myelin disorders. 3rd ed. Berlin: Springer, 2005. p. 37–65.

## Supporting Information

Additional Supporting Information may be found in the online version of this article:

**Data S1.** Supplementary methods.
**Figure S1.** Intramolecular base-pairing interaction in the predicted secondary *PLP1* structures.
**Table S1.** MRI characteristics.
**Table S2.** Clinical characteristics.
**Table S3.** Quantitation of predicted intramolecular base-pairs at the *PLP1* splice donor site in normal and mutant *PLP1* mRNA.

 